CSIRO PUBLISHING

International Journal of Wildland Fire **2012**, *21*, 882–893
http://dx.doi.org/10.1071/WF10116

Linking complex forest fuel structure and fire behaviour at fine scales

E. Louise Loudermilk[A,I], *Joseph J. O'Brien*[B], *Robert J. Mitchell*[C], *Wendell P. Cropper, Jr*[D], *J. Kevin Hiers*[E], *Sabine Grunwald*[F], *John Grego*[G] *and Juan C. Fernandez-Diaz*[H]

[A]School of Natural Resources and Environment, University of Florida, PO Box 110410, Gainesville, FL 32611, USA.
[B]USDA Forest Service, Center for Forest Disturbance Science, Forestry Sciences Laboratory, 320 Green Street, Athens, GA 30602, USA.
[C]Joseph W. Jones Ecological Research Center at Ichauway, 3988 Jones Center Drive, Newton, GA 39870, USA.
[D]School of Forest Resources and Conservation, University of Florida, PO Box 110410, Gainesville, FL 32611, USA.
[E]Eglin Air Force Base, Natural Resource Branch, 107 Highway 85 North, Niceville, FL 32578, USA.
[F]Soil and Water Science Department, University of Florida, PO Box 110290, Gainesville, FL 32611, USA.
[G]Department of Statistics, University of South Carolina, 1523 Greene Street, Columbia, SC 29208, USA.
[H]Geosensing Engineering and Mapping Center, University of Florida, PO Box 116580, Gainesville, FL 32611, USA.
[I]Corresponding author. Present address: Department of Environmental Science and Management, Portland State University, PO Box 751, Portland, OR 97207, USA.
Email: louise.loudermilk@gmail.com

Abstract. Improved fire management of savannas and open woodlands requires better understanding of the fundamental connection between fuel heterogeneity, variation in fire behaviour and the influence of fire variation on vegetation feedbacks. In this study, we introduce a novel approach to predicting fire behaviour at the submetre scale, including measurements of forest understorey fuels using ground-based LIDAR (light detection and ranging) coupled with infrared thermography for recording precise fire temperatures. We used ensemble classification and regression trees to examine the relationships between fuel characteristics and fire temperature dynamics. Fire behaviour was best predicted by characterising fuelbed heterogeneity and continuity across multiple plots of similar fire intensity, where impacts from plot-to-plot variation in fuel, fire and weather did not overwhelm the effects of fuels. The individual plot-level results revealed the significance of specific fuel types (e.g. bare soil, pine leaf litter) as well as the spatial configuration of fire. This was the first known study to link the importance of fuelbed continuity and the heterogeneity associated with fuel types to fire behaviour at metre to submetre scales and provides the next step in understanding the complex responses of vegetation to fire behaviour.

Additional keywords: fuel heterogeneity, IR imagery, LIDAR, longleaf pine, regression tree, savanna.

Received 18 October 2010, accepted 21 February 2012, published online 26 July 2012

Introduction

Savannas are often dependent on frequent fire to maintain their physiognomy and these ecosystems, when frequently burned, are of global importance in sustaining biodiversity (Bond *et al.* 2005). They also are critical in maintaining ecosystem services, such timber, and fuel for energy and grazing (McPherson 1997). The productivity and aerial extent of these ecosystems are significant, accounting for 30% of terrestrial global primary production (Grace *et al.* 2006). Understanding the management of fire in these systems is critical to their ecological services.

Predicting the consequences of fire management of these fire-dependent systems requires that we clearly understand the

connection between fuel heterogeneity, variation in fire behaviour and the influence of fire variation on feedbacks in vegetation and thus fuels (Mitchell *et al.* 2009). The dynamics between this heterogeneous fuel environment and the regulation of future vegetation by fire have been referred to as the ecology of fuels (Mitchell *et al.* 2009). This concept emphasises the importance of fuels as a link between the combustion environment and vegetation response. Specifically, it targets a need for better understanding of the ecological significance of fine fuels and quantifying fuels and fire behaviour at the appropriate scale in frequent-fire-dependent ecosystems (Hiers *et al.* 2007; Mitchell *et al.* 2009). The appropriate scale is ultimately determined by the spatial range of inherent variation of both fuels and fire behaviour (Hiers *et al.* 2009; Loudermilk *et al.* 2009). This is characterised by the spatial distribution and arrangement of vegetation fuel types, fuel structure, biomass and condition (e.g. moisture content) as well as the variability associated with neighbourhood relationships (e.g. fuel connectivity). Fuelbeds – defined here as the understorey vegetation and surface fuels that carry fire (DeBano *et al.* 1998) – in frequent-fire systems have previously been described as homogeneous (Ottmar *et al.* 2007). We have recently shown however, that they vary significantly at submetre scales (Loudermilk *et al.* 2009) and fire varies at the same scale (Hiers *et al.* 2009), thus pointing to a need for finer-scale fuel and fire measurements to elucidate the process behaviour of fire. Ground-based LIDAR (Light Detection and Ranging) data provide finer-scale spatial data (at high spatial resolutions) on fuel structure and type than traditional (point intercept) fuel measures (Loudermilk *et al.* 2009). Infrared (IR) thermography also provides a technological solution to increasing finer-scale measurements of fire behaviour (Kennard *et al.* 2005). Combining these emergent technologies provides great promise in measuring fuels and fire in novel ways that may promote greater understanding of relationships and mechanisms of controls. Recent advances in statistics, in the realm of data-mining, facilitate analysis of such large ecosystem datasets with complex non-linear, high-order relationships (Prasad *et al.* 2006; Seni and Elder 2010).

The objective of this study was to accurately measure data on fuels and fire at a finer scale than previously possible and to analyse relationships between fire and fuel characteristics using statistical ensemble trees. The goal was to explore the extent that variation in fuels can explain significant variation in fire behaviour at the submetre scale in frequently burned longleaf pine woodlands.

Methods

Study site

The site was at Ichauway, an 11 000-ha reserve of the Joseph W. Jones Ecological Research Center in Georgia, USA, classified within the Plains and Wiregrass Plains subsections of the Lower Coastal Plain and Flatwoods section (McNab and Avers 1994). The longleaf pine (*Pinus palustris*) sites have a history of dormant-season prescribed fires for at least 70 years every 1 to 3 years. The understorey consisted of wiregrass (*Aristida stricta*), many forb and prairie grass species and hardwood shrubs. The study area had not burned for 1 year.

Data collection

In spring 2007, 20 georeferenced 4×4-m plots were established to measure fuelbed characteristics. Point-intercept (PI) fuel data (169 samples, 0.33-m grid spacing) were recorded using a 5-mm graduated dowel within each plot. At each PI sample, vegetation types, maximum fuelbed and litter depth, and fuel presence or absence were recorded. The georeferenced sampling captured the spatial variation of the fuelbed found within a 16-m^2 area corresponding to the subcentimetre scale three-dimensional (3D) laser data collected from the ground-based LIDAR. Within 2 weeks of field data collection, the Mobile Terrestrial Laser Scanner (MTLS) was used to collect ground-LIDAR data on all 20 plots. Further details of the MTLS and field methods are in Loudermilk *et al.* (2009) and Loudermilk (2010). Fire behaviour was recorded using an FLIR (forward-looking infrared) digital thermal imagery system (FLIR Inc. S60, Boston, MA, USA), with details on data collection and specifications in Appendix 1 and Hiers *et al.* (2009).

Plots were burned during three controlled burns conducted at an operational scale (~70 ha each) using strip head fires on 23 and 27 February and 16 March 2007. A strip head fire was ignited 5 m upwind of each plot with over 100 m separating strip heads from downwind strips when plots were ignited. Plots within a burn unit were burned and sampled from downwind to upwind. Each operational strip head fire was allowed to burn through the plots undisrupted by additional lines of fire (Hiers *et al.* 2009). Mean wind speed and temperature were similar between days, ranging from 1.47 to 2.19 $m\,s^{-1}$ and 19.4 to 22.9°C respectively. The mean plot level wind speed during the fires ranged from 1.1 to 2.9 $m\,s^{-1}$. Relative humidity ranged from 14.9 to 65.9% between days (Appendices 2, 3).

Data processing

The presence or absence data for fuel types collected in the field (PI data) were represented as categorical binary variables (1 = present, 0 = absent) for spatially explicit points (33-cm spacing). These binary variables were used as (12) independent metrics in the statistical analysis. Additionally, a fuel cluster metric represented the spatial arrangement of the various fuel types across plots (details of the analyses are found in Hiers *et al.* 2009). The fuel cluster metric contained 11 clusters.

Processing the laser data entails merging the point clouds from each scan into a common coordinate frame using the *Polyworks* (InnonMetric, Quebec City, QC, Canada), *Quick Terrain Modeller* (Applied Imagery, Silver Spring, MD, USA) and *TerraScan* (Terrasolid, Jyvaskyla, Finland) software. The subset of the point cloud that covers the region of interest (4×4-m plot) was isolated, with processing details found in Loudermilk *et al.* (2009) and Loudermilk (2010). The spatial resolution of all fuel and fire datasets corresponded to the PI data on fuel types (i.e. 33×33 cm). All datasets were scaled to 169 sample points per plot to coincide with the PI measurements, which represented the entire plot, including edges. LIDAR height (z) metrics calculated within each 33×33-cm area (the 'cell') included mean, maximum, variance, kurtosis, skewness, distribution ratio (mean/maximum), sum and spread (maximum minus minimum). Laser point density and LIDAR intensity values were normalised across all plots by dividing each cell's

value by the maximum value across all plots. LIDAR intensity metrics included mean LIDAR intensity and three values that coupled the interaction between volume of fuel (i.e. laser point density) and type (leaf surface area) or condition (moisture) of the fuel (i.e. LIDAR intensity), namely int_{sqrt}, int_{qdrt} and int_{lnr}. See Loudermilk (2010) and Appendix 4 for details.

The FLIR fire images were analysed using FLIR Systems' *ThermaCAM Researcher Pro* version 2.7 software. The images were rectified and georeferenced using image processing software (*Geomatica*, PCI Geomatics, Alexandria, VA). Summary statistics over time consisted of four fire behaviour metrics (Tmax, maximum temperature; Q90, 90th quantile temperature; T300, residence time above 300°C; and T500, residence time above 500°C). Tmax was the highest temperature measured within an area. Q90 filtered out the often short-term flaming front and helped distinguish unburned patches from low-temperature glowing-phase fire (Hiers *et al.* 2009). The two residence time variables potentially segregated flaming-phase fire-intensity measurements (T500) from the combined smouldering and flaming phases (T300). Appendix 4 includes all fuelbed and fire metrics used in this analysis.

Grouping of plots

Plots were grouped based on their fire behaviour metrics using k-means clustering with *SAS v9.1* (SAS Institute Inc., Cary, NC, USA). This reduced discrepancies associated with local weather or fuel condition variability. The number of clusters was chosen based on the Cubic Clustering Criterion and pseudo *F* statistic. There were three distinct clusters among the plots, representing three levels of fire intensity. There was no distinction between the three fire groups based on particular day of burn, plot-level wind speed (range = 1.79–1.85 m s^{-1}) or ambient temperature (19.4 to 22.9°C). Although relative humidity was different between days (i.e. variable within groups), there was most likely little to no variability in relative humidity at the plot level for influencing fire behaviour (i.e. 3–5-min fire duration). Details are in (Loudermilk 2010) and Appendix 2,3.

Regression-tree modelling

Regression-tree modelling provides an alternative approach to multiple regression, designed specifically for complex non-linear relationships (Breiman *et al.* 1984). The *CART* (Classification and Regression Tree) software (v. 5.0, Salford Systems, San Diego, CA) partitions variation in a binary recursive approach. This iteratively creates relatively homogeneous (low-deviation) terminal nodes, which then define their predictive ability (Grunwald *et al.* 2009). Recent advances in data mining include ensemble tree methods, which optimise target and predictor variable fitting (Seni and Elder 2010). We found other linear ordination methods (e.g. correlation matrix, linear regression) ill-suited for describing the multifaceted associations between fine-scale fuels and fire behaviour. *CART* has the ability to overcome the deficiencies of traditional linear methods and often provides superior results, especially when multiple cross-validation procedures are used (Lewis 1992). Many environmental datasets are complex, with high-order interactions that may not be easily modelled using traditional multiple regression analysis. Ensemble trees are specifically designed for handling these problems (Breiman *et al.* 1984; Prasad *et al.* 2006).

The LIDAR metrics and fuel types were analysed using each of the four fire behaviour metrics with least-squares regression-tree modelling in *CART*. *CART* analysis was run for each grouped dataset (mid-range (nine plots), high-range (five plots) and low-range (six plots)) characterised by distinct differences in fire behaviour and three randomly chosen plots within each group (three plots). Spatial coordinates (x, y) were incorporated into one fire metric model within each of the three individual plots to assess the influence of spatial configuration of a plot-level fire. A total of 27 *CART* simulations were run. Using the ensemble tree methodology, committees trees (CT) in ARCing mode (Adaptive Resampling and Combining) were used in *CART*. The strength of running the CT in ARCing mode is its ability to run multiple (often hundreds of) regression trees and learn from each tree, based on probability of bootstrap selection. This ultimately builds a stable CT model where predicted values are averaged across multiple versions of the predictors. Detailed descriptions of each regression-tree methodology, including statistical aspects, are found elsewhere (Breiman *et al.* 1984; De'ath and Fabricius 2000; Prasad *et al.* 2006; Grunwald *et al.* 2009).

One hundred trees were run per CT simulation, while employing the 10-fold cross-validation procedure in *CART* to test prediction performance and optimise tree size (i.e. control overfitting). The cross-validation approach is in essence a 'repeated independent validation' of the model where 10% of the data is withheld for testing (model verification) and the remaining 90% is used to predict the response variable. This process is repeated and average error metrics are calculated for prediction performance. This multiple continuous cross-validation procedure minimises biases resulting from a single-validation procedure (Lewis 1992; Power 1993; Rykiel 1996; Sargent 2005). All trees are pruned and thus optimised (minimum cross-validation relative error) to avoid overfitting, because the strategy is to find a parsimonious tree that predicts well, with the fewest input variables (Breiman *et al.* 1984). No variables were removed from any models in our optimisation approach, allowing a comparative analysis between fire models with the same set of fuel variables both across (grouped) and between (individual) plots. For each model, the coefficient of determination (R^2), root-mean-square error (RMSE), residual prediction deviation (RPD), cross-validation relative error (CVRE), resubstitution relative error (RRE) and number of terminal nodes (T_n) (De'ath and Fabricius 2000; Grunwald *et al.* 2009; Vasques *et al.* 2009) were recorded.

The *CART* relative importance rankings (importance value (IV)) were used to assess the ability of the fuel metrics to predict each of the fire metrics across the 27 model runs. Whereas model fit and error statistics provided overall model evaluation, these IVs allowed us to assess the relative explanatory power (ranging from 0 to 100) of the metrics in a heterogeneous fire environment.

Results and discussion

Fire intensity groups

Relationships between fine-scale fuelbed and fire behaviour characteristics were strong, especially when the fire environment

Table 1. Results of CART analysis for each grouped dataset using the 10-fold cross-validation procedure

Residence times (T300, T500) are in number of 4-s intervals. Response variables are the fire metrics, namely Tmax, maximum temperature (°C); Q90, 90th quantile temperature (°C); T300, residence time above 300°C; T500, residence time above 500°C. T_n, number of terminal nodes; CVRE, cross-validation relative error; RRE, resubstitution relative error; R^2, coefficient of determination; RMSE, root-mean-square error; RPD, residual prediction deviation

Response variable	T_n	CVRE	RRE	R^2	RMSE	RPD
High-range fire group (five plots, $n = 845$)						
Tmax	136	0.57	0.10	0.80	23.52	2.25
Q90	132	0.42	0.08	0.88	24.24	2.86
T300	95	0.18	0.05	0.88	0.97	2.92
T500	122	0.32	0.08	0.83	0.60	2.41
Mid-range fire group (nine plots, $n = 1521$)						
Tmax	236	0.54	0.11	0.78	26.85	2.14
Q90	218	0.52	0.12	0.79	22.54	2.16
T300	219	0.40	0.08	0.83	0.91	2.40
T500	243	0.60	0.14	0.78	0.50	2.08
Low-range fire group (six plots, $n = 1014$)						
Tmax	128	0.46	0.11	0.83	33.30	2.43
Q90	140	0.28	0.08	0.86	8.80	2.30
T300	152	0.32	0.09	0.80	0.90	2.18
T500	150	0.43	0.09	0.79	0.37	2.11

was categorised *a priori* using fire intensity groups (Table 1, Fig. 1). Other studies have used ground (Hopkinson *et al.* 2004; Loudermilk *et al.* 2009) and aerial LIDAR (Lefsky *et al.* 1999; Hall *et al.* 2005) as well as intensive field inventory data (Brown 1974, 1981) to characterise forest fuels and structure, but this analysis is the first to relate complex fuelbed structure and types to specific fire behaviour attributes at submetre scales.

Grouped fire models (low-, middle- and high-range data) performed well ($R^2 = 0.78$ to 0.88, RPD = 2.11 to 2.92, Table 1, Fig. 1) and often better than individual plot models ($R^2 = 0.60$ to 0.84). Grouped fire models exhibited strong model fit, with high R^2 values ($R^2 = 0.78$ to 0.88), low error (e.g. RRE = 0.051 to 0.141) and RPD values above 2 (RPD = 2.11 to 2.92). Reduction in dimensionality through fire behaviour grouping allowed optimised predictions of the response variables (Tmax, Q90, T300 and T500). The three groups separated variability of fire behaviour, therefore optimising variability of fuel characteristics within each group. Modelling the collective dataset (all 20 plots) demonstrated weaker relationships (Appendix 5) than when separating by fire behaviour intensity (Table 1).

The T300 and Q90 were especially strong variables in middle- and high-range fire groups (T300 RPD = 2.40, 2.92; Q90 RPD = 2.16, 2.86, Table 1, Fig. 1). In the low-range group, Tmax was the strongest model (RPD = 2.43). In this group, temperature variability and intensity were lower (data not

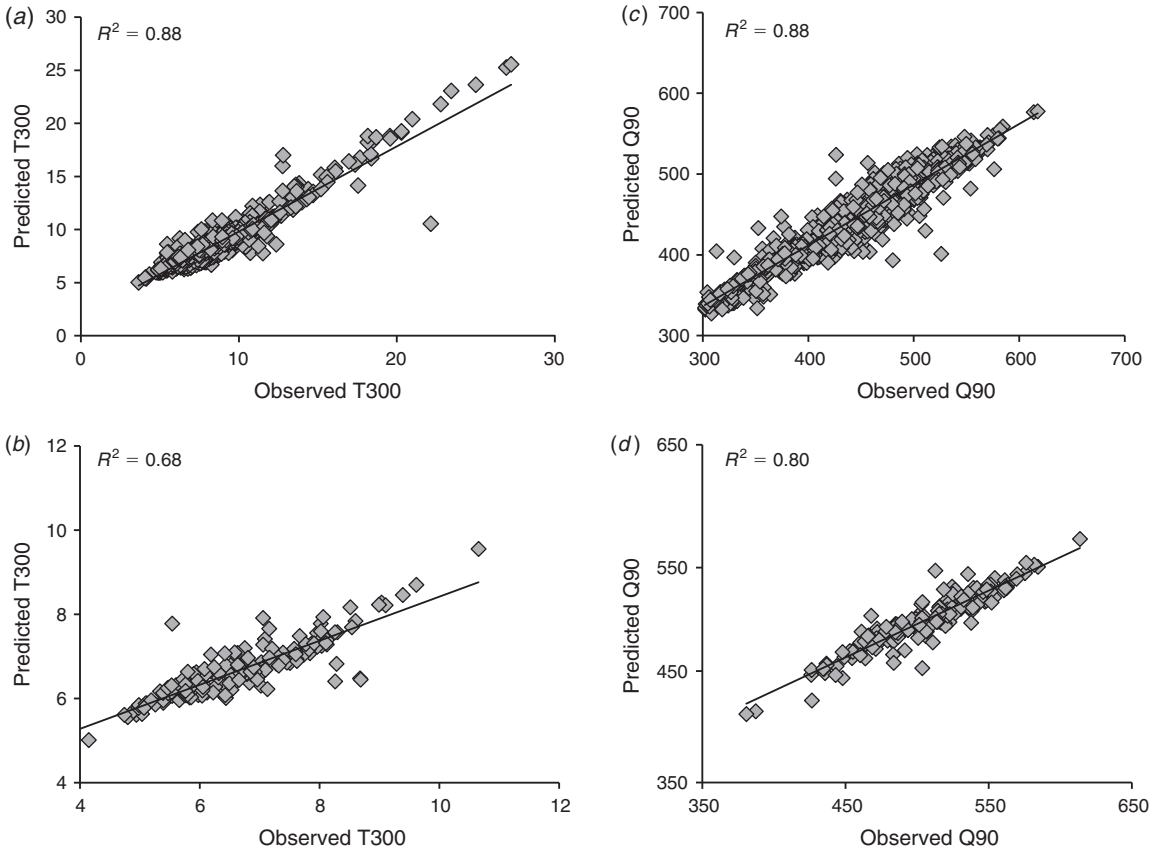

Fig. 1. Regression-tree results using CART (classification and regression trees) for Q90 (90th quantile temperature) and T300 (residence time (4-s intervals) above 300°C) using the high-range fire group (five plots, $n = 845$, (*a*), (*c*)), and individual plots within the high-range fire group ($n = 169$, (*b*), (*d*)). Note the change in scale for the individual plots.

Table 2. Top five importance value (IV) rankings of input variables from CART analysis at the grouped-level analysis

Residence times (T300, T500) are in number of 4-s intervals. Complete list of input variables (metrics) is found in Appendix 4. Tmax, maximum temperature (°C); Q90, 90th quantile temperature (°C); ht, height; ht dist. ratio, height distribution ratio (mean/maximum); int_{lnr}, sum of normalised LIDAR intensity values; int_{qdrt} and int_{sqrt}, sum of normalised intensity values scaled by the quadratic and square root function

Response variables	Top five ranked fuel metrics (IV)
High-range fire group (five plots, $n = 845$)	
Tmax	Spread of hts (100), max ht (96.3), sum of hts (81.2), mean ht (81), point density (75.5)
Q90	Fuel clusters (100), mean ht (73.3), point density (61.7), sum of hts (54.8), spread of hts (53.8)
T300	Mean LIDAR intensity (100), ht dist. ratio (66.5), fuel clusters (66.3), int_{lnr} (40.8), int_{qdrt} (39.4)
T500	Sum of hts (100), mean ht (97.9), ht dist. ratio (96.7), point density (69.4), max ht (66.0)
Mid-range fire group (nine plots, $n = 1521$)	
Tmax	Mean ht (100), ht variance (96.5), sum of hts (82.1), ht kurtosis (81.9), ht skewness (78.3)
Q90	Spread of hts (100), max ht (85.3), ht variance (79.1), ht dist. ratio (74.4), ht skewness (74.2)
T300	Mean ht (100), ht variance (78.2), ht kurtosis (71.0), ht dist. ratio (45.6), spread of hts (42.6)
T500	Mean ht (100), ht variance (96.8), int_{sqrt} (88.4), mean LIDAR intensity (82.8), spread of hts (80.2)
Low-range fire group (six plots, $n = 1690$)	
Tmax	Mean LIDAR intensity (100), mean ht (72.1), ht skewness (72.1), spread of hts (68.5), Fuel clusters (64.8)
Q90	Ht variance (100), max ht (86.3), spread of hts (83.6), mean ht (81.1), ht dist. ratio (59.8)
T300	Ht kurtosis (100), ht skewness (86.0), mean ht (78.5), int_{qdrt} (76.1), sum of hts (72.9)
T500	Mean ht (100), ht variance (73.2), max ht (73.0), spread of hts (70.1), sum of hts (62.9)

shown). Modelling Q90 may be most appropriate when analysing plots with similar fire characteristics, where there is sufficient, yet distinguishable variability in temperature and fuel attributes. The T500 models may be best suited for higher intensity fires (e.g. high-range fire group T500, RPD = 2.41), where there are adequate samples (i.e. 33×33-cm cells) flaming at or above 500°C.

Each *CART* model was unique in terms of sensitivity to particular fuel types and characteristics, often varying between fire intensity groups. Mean fuelbed depth (LIDAR height) was a significant driver for all models (including grouped and individual plot models) (Table 2). Twenty-one of the 27 models had mean LIDAR height within the top-five ranked variables. Other height and fuelbed metrics varied by group in response to changes in fuelbed continuity. Variability in fuelbed depth was a strong predictor for the middle- and low-range fire models, whereas sum of heights, point densities and fuel clusters were more prominent in the high-range fire models. The skewness and kurtosis metrics reflected fuels that were distributed towards the shorter or taller vegetation or those that were excessively peaked (or lacking a peak) around the mean height respectively. Disruption in fuelbed continuity (Fig. 2) causes variability in radiative and convective heat transfer rates between neighbouring fuels at small horizontal scales (<1 m), influencing fire intensity values (DeBano *et al.* 1998). As fuel becomes more spatially uniform (Fig. 2), so do heat-transfer mechanisms driving small-scale fire intensity.

Maximum height values were more important for temperature than residence time within all fire groups. Maximum fuelbed height within cells (amount of fuel available to burn) directly impacts fire temperature (Whelan 1995). Residence time is influenced by bulk density and specific fuel types, such as downed woody debris that may cause extended smouldering. Temperatures may be similar with or without the downed woody debris, but residence time increases substantially (Mitchell *et al.* 2009).

LIDAR intensity metrics were important drivers among models. Mean intensity was the most important metric (no. 1 in IVs) for T300 and Tmax in the high- and low-range fire groups respectively (Table 2). The int_{sqrt} and int_{qdrt} metrics were significant drivers for T500 (no. 3 IV, middle-range group) and T300 (no. 4 IV, low-range group). Otherwise, all intensity variables had moderate IVs with no distinct trends between models or groups. The difficulty in using LIDAR intensity values in relation to fuels is that intensity values represent target surface reflectance coupled with size of the intercepted surface. These are difficult to separate and quantify (Riaño *et al.* 2004). The point-intercept fuel-cluster metric was a significant model driver among all fire group models. Within the high-range fire group, the fuel-cluster metric was the most significant driver for Q90 (no. 1 IV) and for T300 (no. 3 IV) (Table 2). Their considerable model strength (RPD = 2.86–2.92) coupled with their significant correlation with the fuel clusters supports the findings in Hiers *et al.* (2009) that Q90 was more sensitive to fuel clusters than the other fire metrics. A stronger fuel distinction represented variability in fire behaviour, particularly smouldering effects. Conversely, the fuel clusters were more predictive for Tmax than Q90 in the middle- (nos 7 and 14 IV) and low-range (nos 5 and 14 IV) fire groups. Impacts of fuelbed continuity were diminished in lower-intensity groups and the fuel clusters coupled with structure influenced temperature variability. The categorical fuel-cluster variables were significant among the fire group models and often outperformed many of the continuous LIDAR variables.

Fuel types were distinguishable between the fire groups. The most prominent fuel-type metrics within each model ranged in IVs from 5.4 to 27.0 in the fire groups. Wiregrass was a comparatively stronger driver in the high-range fire groups (maximum IV = 21.6). Bare soil was a dominant fuel-type metric for Tmax for both high- (IV = 9.0) and middle-range (IV = 13.3) fire groups as well as T500 (IV = 6.4, low group). Residence time was more sensitive to areas of bare soil than

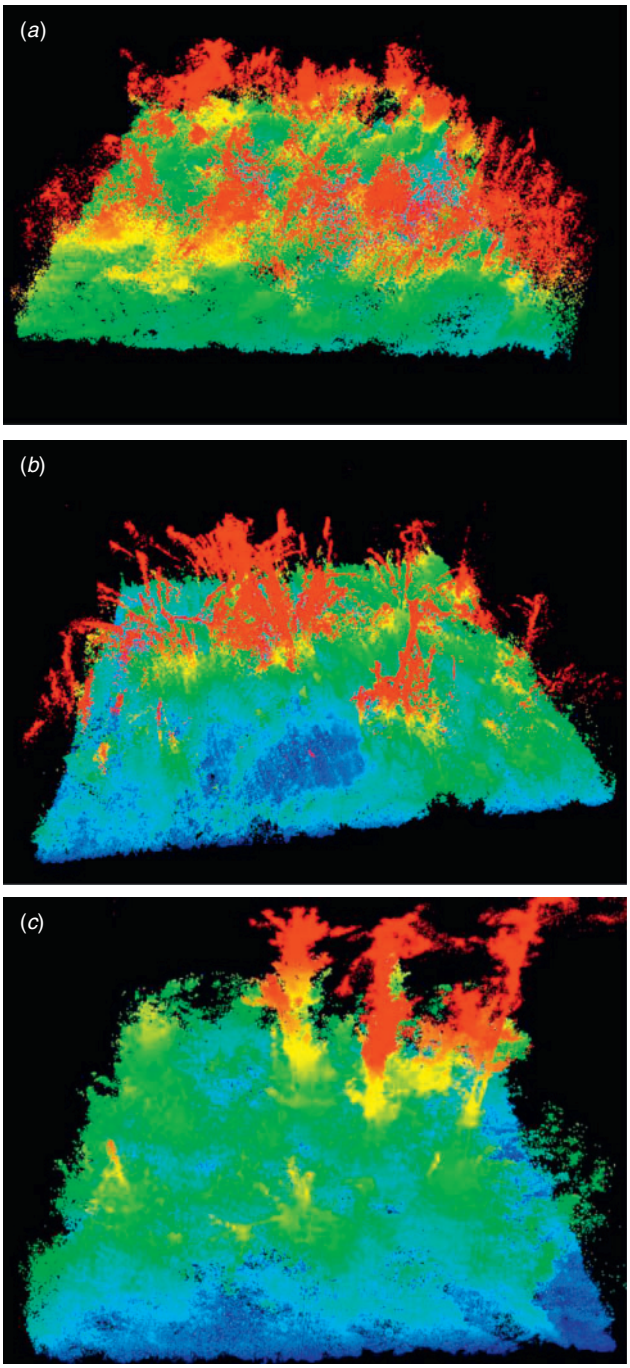

Fig. 2. Changes in fuelbed continuity among the three plots (4 × 4 m) modelled individually, namely (*a*) the high-range plot (maximum height: 1.5 m); (*b*) the middle-range plot (maximum height: 1.5 m); and (*c*) the low-range plot (maximum height: 3.9 m). Note the loss in horizontal and vertical connectivity and increase in patchiness of fuels from the high-range to low-range plot ((*a*) to (*c*)). The colour gradient represents vegetation height distribution, which aids in visualisation of the 3D vegetation structure.

temperature. Maximum temperature readings could be influenced by bare soil in especially high-intensity fire areas, where fluctuations in temperature were most likely higher. Although pine litter was a less significant driver, it was notable that the

Table 3. Results of CART analysis for individual plots ($n = 169$ each) within the three fire groups, including those with *x*, *y* coordinates included as inputs

Residence times (T300, T500) are in number of 4-s intervals. Tmax, maximum temperature (°C); Q90, 90th quantile temperature (°C); T_n, number of terminal nodes; CVRE, cross-validation relative error; RRE, resubstitution relative error; R^2, coefficient of determination; RMSE, root-mean-square error; RPD, residual prediction deviation

Response variable	T_n	CVRE	RRE	R^2	RMSE	RPD
High-range individual plot						
Tmax	27	0.46	0.06	0.81	23.08	2.27
Q90	25	0.51	0.12	0.80	17.74	2.26
T300	24	0.40	0.11	0.68	0.64	1.78
T300 (*x*, *y*)	25	0.44	0.11	0.74	0.58	1.95
T500	29	0.60	0.10	0.76	0.44	2.03
Middle-range individual plot						
Tmax	25	0.57	0.12	0.74	27.95	1.95
Q90	22	0.65	0.13	0.64	30.34	1.66
Q90 (*x*, *y*)	21	0.52	0.16	0.72	27.10	1.86
T300	25	0.48	0.11	0.60	1.54	1.58
T500	27	0.44	0.12	0.61	0.72	1.59
Low-range individual plot						
Tmax	25	0.40	0.10	0.79	37.02	2.20
Tmax (*x*, *y*)	25	0.32	0.09	0.84	33.20	2.45
Q90	19	0.41	0.09	0.75	7.80	1.71
T300	24	0.61	0.19	0.70	0.74	1.81
T500	13	0.67	0.28	0.76	0.33	2.01

litter and perched litter abundance was directly related to the associated fire group. For instance, the abundance of pine litter and perched pine litter was highest in the high-range fire group (e.g. 69 and 47%, compared with 38 to 50% and 32 to 34% for other groups). The variability in pine litter was likely less influential in groups because the variability was dissipated by clustering the plots by fire intensity. Interestingly, pine litter abundance was more influential at the collective level (i.e. modelling all plots together; data not shown, but see Loudermilk 2010). Relative to other fuel types, pine-litter abundance and distribution dominantly impact fire intensity within this system, with their high surface area-to-volume ratio and high resin content (Hendricks *et al.* 2002). This fuel type, however, cannot be accurately measured with LIDAR instrumentation because of its implicit structure within the fuelbed and compaction near the ground. As surface leaf litter, it is virtually indistinguishable from LIDAR returns of the ground. Similarly, perched pine needles are draped over plants, becoming a part of their architecture. The clustering of fuels was the most effective approach to capturing the complex heterogeneity in fuel types for fire behaviour analysis.

Individual plots

Individual plot analysis of fine-scale fire events, minimally influenced by local weather or fuel state, was useful. The mean wind-speed values within the three individual plots ranged between 1.2 and 2.0 m s^{-1}. All models were strong ($R^2 = 0.60$ to 0.84, RPD = 1.58 to 2.27, Table 3). The individual high-range plot (Table 3, Fig. 1) generally performed better than the middle- or low-range group, similarly to the grouped data findings.

Table 4. Top five importance value (IV) rankings of input variables from CART analysis at the individual plot level

Temperatures (Tmax, Q90) are in °C. Residence times (T300, T500) are in number of 4-s intervals. Complete list of input variables (metrics) is found in Appendix 4. ht, height; ht dist. ratio, height distribution ratio (mean/maximum); int_{lnr}, sum of normalised LIDAR intensity values; int_{qdrt} and int_{sqrt}, sum of normalised intensity values scaled by the quadratic and square-root function

Response variables	Top five ranked fuel metrics (IV)
High-range plot ($n = 169$)	
Tmax	Point density (100), int_{sqrt} (81.8), int_{lnr} (81.3), sum of hts (60.1), int_{qdrt}(57.6)
Q90	spread of hts (100), sum of hts (87.2), ht dist. ratio (77.2), point density (76.8), int_{lnr} (66.8)
T300	Point density (100), int_{lnr} (91.8), int_{qdrt} (85.9), int_{sqrt} (82.8), mean ht (46.4)
T300 (x, y)	Ht variance (100), point density (97.3), int_{qdrt} (89.9), spread of hts (79.9), y coordinate (78.9)
T500	Ht dist. ratio (100), ht kurtosis (86.7), point density (79.6), mean ht (67.9), ht variance (67.5)
Mid-range plot ($n = 169$)	
Tmax	Sum of hts (100), mean ht (91.3), ht skewness (66.2), point density (64.9), ht variance (44.9)
Q90	Max ht (100), mean LIDAR intensity (93.9), mean ht (88.3), spread of hts (79.4), sum of hts (77.7)
Q90 (x, y)	y coordinate (100), mean LIDAR intensity (90.7), ht skewness (71.6), max ht (68.3), spread of hts (66.1)
T300	Ht dist. ratio (100), point density (96.3), spread of hts (82.4), mean ht (76.4), int_{lnr} (74.3)
T500	Ht variance (100), ht dist. ratio (76.0), ht skewness (74.4), ht kurtosis (71.2), spread of hts (65.7)
Low-range plot ($n = 169$)	
Tmax	Mean ht (100), spread of hts (87.0), max ht (77.9), ht kurtosis (69.0), ht skewness (60.6)
Tmax (x, y)	x coordinate (100), ht kurtosis (58.8), ht skewness (57.7), spread of hts (49.2), int_{lnr} (48.8)
Q90	Mean ht (100), point density (65.5), ht variance (62.8), sum of hts (59.7), max ht (57.8)
T300	Mean ht (100), sum of hts (67.4), mean ht (62.6), int_{sqrt} (60.1), int_{qdrt} (56.1)
T500	Ht skewness (100), mean ht (98.4), ht kurtosis (76.0), mean LIDAR intensity (61.9), ht dist. ratio (53.0)

Results were less consistent than between the grouped models, and model fit was often worse than for the grouped data: only five of the model runs had RPD values above 2. This may be explained by the model sensitivity to extreme values. When other plots had comparable outliers, especially within a characteristic fire group, then the variability was smoothed, improving predictive models. Stronger statistical models were found using grouped fire-trait data, whereas model strength of individual plots varied considerably depending on the local fuel, weather and fire environment.

Variability between plots was evident when examining the predictive power of the fuel metrics (Table 4). Mean fuelbed depth (LIDAR height) was one of the strongest drivers. In the low-range plot, it ranked within the top three IVs for all models. Point density was a strong driver for all models in the high-range fire plot (within top five ranked IVs), similarly to the grouped results. Point density (and sum of heights) was stronger in the lower-intensity plots than within the grouped results. This finding suggests that fuelbed continuity may be more sensitive at the plot level. The two models for T500 were consistent with the middle and low ranges in relation to point density and height distribution metrics. The high-range plot displayed fuels that had few disruptions in fuelbed structure and heights across the plot (Fig. 2*a*). The fuelbed was patchier within the middle-range plot (Fig. 2*b*), whereas large variations in height and patchy fuels were found in the low-range plot (Fig. 2*c*). This provides further support that fine-scale spatial fuelbed structure significantly influenced fire behaviour within and between plots.

LIDAR intensity metrics were moderate to high predictors across all plots (Table 4), signifying their utility as a fuel metric for fire behaviour modelling. Seven of the twelve individual models (without x, y) had at least one LIDAR metric within the top five IVs, but mechanistic explanation of the LIDAR intensity associations needs additional development.

Bare soil (<1% abundance of all fuel types) was important for residence time, which was only distinguishable in the grouped-level analysis using the PI fuel-cluster metric. For the high-range plot, the bare-soil metric (no. 8 IV) was especially strong for T300, outperforming various LIDAR height metrics. The 10- and 100-h fuel metrics were more influential at the plot level, also demonstrating significance of both Q90 and residence time.

Spatial configuration was an important predictor of fire behaviour (Table 3, initial RPD = 1.66 to 2.20 without geographic coordinates and improved RPD = 1.86 to 2.45 with geographic coordinates). The improvement from including fuel spatial positions was largest for initially weaker models (e.g. Q90, RPD improved from 1.66 to 1.86 and R^2 from 0.64 to 0.72), where wind direction or neighbourhood fuel combustion properties could influence fire behaviour more than fuel structure and type alone. The spatial metric was found in the top five IVs for all three (x, y) models (Table 4), which changed the predictive ability (IVs) of some other variables. This caused a 'spatial masking' of certain fuel characteristics. For instance, the significance of bare soil in the T300 model decreased in the T300 (x, y) model (i.e. bare soil IV changed from no. 8 (35.8) to no. 15 (19.9)). This also caused interactions with other fuel characteristics. Deciduous oak litter was not a predictor for Q90 without including x, y values (i.e. IV ranking changed from no. 17 (0) to no. 12 (17.1)), becoming the most significant fuel-type metric. The same occurred for forbs in the Tmax (x, y) model. Similarly, some LIDAR metrics, such as height variance in the T300 model, significantly increased in importance. Some metrics were more consistent (e.g. point density and int_{qdrt} for T300, mean LIDAR intensity for Q90). These results signify

sensitivity to the spatial configuration of fire movement between fuels. We also modelled the spatial autocorrelation of the residuals; however, very weak spatial autocorrelations were found, warranting no further modelling of spatial autocorrelation patterns.

Constraints of the analyses

The non-linear approach used in this study, though novel, has constraints. Common fuel measurements (e.g. fuel moisture and biomass) often used in relating fuels to fire behaviour were not used in this study. In all likelihood, fuel moisture was relatively constant during the 3- to 5-min fires, eliminating the need to incorporate within-plot fuel moisture conditions. The fuel-cluster metric, used in the fire group models, accounted for variation in fuel moisture content between similar fire-intensity plots. In addition, certain LIDAR metrics may represent biomass; a particular fuel's laser point-density is likely proportional to volume and highly correlated with biomass and leaf area (Loudermilk *et al.* 2009).Testing the significance of biomass and other environmental variables may be useful. LIDAR does not directly distinguish between vegetation types. Height thresholds have been used to classify the understorey and overstorey (Riaño *et al.* 2003). Tree species have been differentiated by individual tree canopy shape and size or when coupled with remotely sensed imagery (Popescu *et al.* 2004). LIDAR intensity values have been used to distinguish between fuel types by variation in leaf area and vegetation height (Su and Bork 2007; Wing *et al.* 2010), but vegetation types within the surface fuelbed cannot be easily determined. Despite these potential caveats, this statistical approach is promising for addressing fuel–fire relationships at this scale that are otherwise difficult to assess empirically.

IR thermography was critical for enabling us to capture spatially explicit fire behaviour to link with fuel structure and type. Whereas flame characteristics are frequently used as dependent variables in fire behaviour analysis, the system we used only records temperatures of surfaces, i.e. living and dead vegetation and soil. The system does not capture flame characteristics well; in fact, emission from the surfaces of particles entrained in combusting gases is the main source of IR radiation detected by the S60. If we had chosen to capture flame characteristics such as flame length, we would have had to rely on subjective and error-prone visual estimates. As our ultimate goal was to link fuels to fire behaviour and eventually fire effects, we focussed on capturing the temperatures of fuel surfaces and non-combusting vegetation and soil, which are variables closely linked to both fire behaviour and fire effects. Although inaccuracy could have been introduced by the camera position and the impacts of atmospheric absorption and transmittance, the S60 IR wavelengths greatly reduce errors from atmospheric emission and absorption. Soot particles dominate flame IR emission in this system and errors associated with flame emission would also be relatively minor as flames flicker and soot becomes diluted rapidly with distance from the fuel (Dupuy *et al.* 2007). Unburned fuels between the camera and fire would also introduce error, but the angle view of the camera (40°) and the grassy fuels with scattered shrubs minimised this error. Furthermore, the position of the camera upwind and perpendicular to the flaming front also reduced the potential for unburned fuels blocking burning fuels. The cumulative effects of these errors would only minimally reduce the predictive power of the models. Although no measurement system is perfect, we argue that the spatially explicit measurements made possible by IR thermography are superior to any currently available technology. Thermocouples and temperature-sensitive paints and other currently available methods are even more error-prone and cannot capture fine-scale spatial data effectively (Kennard *et al.* 2005).

Qualitative observations indicate that differences in fire behaviour among fuels cells diminish at higher intensities. Gusty winds were observed to change both the intensities that some fuel cells burned at and the behaviour of the fireline among neighbourhoods of different cells. Determining whether the relationship between fire intensity and fuel characteristics is continuous or shows a threshold response would be a useful avenue of research.

Implications

This study is another step in understanding the complex responses of vegetation to fire behaviour and establishing the concepts of the ecology of fuels (Mitchell *et al.* 2009) and wildland fuel cells (Hiers *et al.* 2009). Both concepts address the inability of past approaches to fully connect fuel heterogeneity to fire behaviour and fire behaviour to fire effects.

Forest vegetation dynamics of fire-dependent systems, particularly longleaf woodlands, are a function of competition and fire (Pecot *et al.* 2007; Loudermilk *et al.* 2011). Both processes regulate the types, amounts and spatial distribution of fuels (Mitchell *et al.* 2009). We have previously shown that small-scale variation in vegetation impacts fuel types and amounts (Loudermilk *et al.* 2009), and the variation in fuel cells influences the spatial patterns in fire (Hiers *et al.* 2009). Hiers *et al.* (2009) found that fuel and fire heterogeneity were similar at these fine scales, where discrete patches of each could be determined (using the IR imagery and ground-based LIDAR), and discussed the complexity of their relationships at this scale. The present work advances the previous study (Hiers *et al.* 2009) significantly by directly linking specific fine-scale fuel characteristics, e.g. fuel depth, fuel type, spatial configuration, to particular fire behaviour attributes within and between individual fires (i.e. 4×4-m plots).

This study also has implications for ecosystem management and ecological forestry silvicultural prescriptions. Fine fuels, in this case pine-needle litter, drive fire dynamics within a longleaf pine system by supplying a continuous flammable fuelbed. Timber extraction disrupts (among other things) the subsequent distribution and abundance of pine litter, contributing to negative feedbacks between fuel continuity and fire behaviour. The responses to the small-scale heterogeneity in the fuelbed are relatively unknown and could be examined through these techniques. Natural pine regeneration response to subsequent vegetative competition (i.e. established hardwoods) in newly created forest gaps (i.e. from individual or group-selection techniques) is critical. The competitive (or possible facilitative) interactions between established pine seedlings and hardwood sprouts may be determined by the spatial and temporal changes

in fuels (impacted by overstorey removal) that ultimately drive changes in fire behaviour (Mitchell *et al.* 2006; Pecot *et al.* 2007). This fine-scale assessment of fuel and fire variability has often been ignored; first, because of measurement constraints and second, because of a misconception that low-intensity fires occurring under similar weather conditions and general fuel traits in these systems are relatively homogeneous and within-plot variability was insignificant for driving fire effects. Although this may be true at a particular scale beyond plot level, the finer-scale variability has been neglected and its implications at other scales need to be investigated.

These low-intensity surface fuel–fire concepts are scale-less and can be applied to any-size fire where fuel composition and structure may drive combustion and smouldering characteristics associated with low-intensity wildland fires. Although low-intensity controlled burns are often applied when wind speeds are low ($\sim$0.5–1.5 m s^{-1}) and other environmental variables are optimal (temperature, relative humidity, wind direction; Wade *et al.* 1989), the natural fire regime in these pinelands is characteristically high-frequency low-intensity, where these surface fuel–fire concepts are relevant. These low-intensity fires are characteristic of south-eastern USA pinelands (Smith *et al.* 2009) and shape savanna systems globally (Bond *et al.* 2005).

Conclusions

This study was the first integration of high-resolution LIDAR and thermal imagery to assess fine-scale relationships between fuelbed variation and heterogeneity in fire behaviour. Grouping the plots based on similar fire intensities provided the best models in terms of fit and predictive capability and reduced the effects of plot-to-plot variation in fuel, fire and weather conditions that were not explicitly modelled. The strongest model fit was found in the high-range fire groups, specifically for Q90 and T300, where the fuel clusters were highly significant predictors. Although grouped datasets were most promising, the individual plots revealed significance of specific fuel types (e.g. bare ground, deciduous litter) and the importance of spatial configuration of fuel types. Mean fuelbed height was overall a significant variable, important for temperature and residence time predictions in these fine-fuel-dominated fuelbeds. Fuel metrics demonstrated the importance of fuelbed continuity (both horizontal and vertical) in driving fire behaviour at fine scales. This work offers promise in linking fire behaviour to fire effects at appropriate scales in these ecosystems.

Acknowledgements

We thank the School of Natural Resources and Environment and the School of Forest Resources and Conservation at the University of Florida for providing logistic and financial support throughout this research. We thank the Joseph W. Jones Ecological Research Center for support during research development, field work and final stages of this work. The Ordway–Swisher Biological Station, Melrose, FL, was important for the pilot stage of this work. We thank the USDA Forest Service for research development and logistical support. We thank the National Center for Airborne Laser Mapping at the University of Florida for providing the ground-LIDAR instrumentation (i.e. MTLS) and engineering expertise, with special thanks to K. Clint Slatton.

References

Bond WJ, Woodward FI, Midgley GF (2005) The global distribution of ecosystems in a world without fire. *New Phytologist* **165**(2), 525–538. doi:10.1111/J.1469-8137.2004.01252.X

Breiman L, Friedman JH, Olshen RA, Stone CJ (1984) 'Classification and Regression Trees.' (Wadsworth, Inc.: Belmont, CA)

Brown JK (1974) Handbook for inventorying downed woody material. USDA Forest Service, Intermountain Research Station, Report GTR-INT-16. (Ogden, UT)

Brown JK (1981) Bulk densities of non-uniform surface fuels and their application to fire modeling. *Forest Science* **27**, 667–683.

De'ath G, Fabricius KE (2000) Classification and regression trees: a powerful yet simple technique for ecological data analysis. *Ecology* **81**(11), 3178–3192. doi:10.1890/0012-9658(2000)081[3178:CARTAP]2.0.CO;2

DeBano LF, Neary DG, Ffolliott PF (1998) 'Fire Effects on Ecosystems.' (Wiley: New York)

Dupuy J, Vachet P, Maréchal J, Meléndez J, de Castro AJ (2007) Thermal infrared emission–transmission measurements in flames from a cylindrical forest fuel burner. *International Journal of Wildland Fire* **16**(3), 324–340. doi:10.1071/WF06043

Grace J, José JS, Meir P, Miranda HS, Montes RA (2006) Productivity and carbon fluxes of tropical savannas. *Journal of Biogeography* **33**(3), 387–400. doi:10.1111/J.1365-2699.2005.01448.X

Grunwald S, Daroub SH, Lang TA, Diaz OA (2009) Tree-based modeling of complex interactions of phosphorus loadings and environmental factors. *The Science of the Total Environment* **407**(12), 3772–3783. doi:10.1016/J.SCITOTENV.2009.02.030

Hall SA, Burke IC, Box DO, Kaufmann MR, Stoker JM (2005) Estimating stand structure using discrete-return LIDAR: an example from low-density, fire-prone ponderosa pine forests. *Forest Ecology and Management* **208**(1–3), 189–209. doi:10.1016/J.FORECO.2004.12.001

Hendricks JJ, Wilson CA, Boring LR (2002) Foliar litter position and decomposition in a fire-maintained longleaf pine–wiregrass ecosystem. *Canadian Journal of Forest Research* **32**(6), 928–941. doi:10.1139/X02-020

Hiers JK, O'Brien JJ, Will RE, Mitchell RJ (2007) Forest floor depth mediates understory vigor in xeric *Pinus palustris* ecosystems. *Ecological Applications* **17**(3), 806–814. doi:10.1890/06-1015

Hiers JK, O'Brien JJ, Mitchell RJ, Grego JM, Loudermilk EL (2009) The wildland fuel cell concept: an approach to characterize fine-scale variation in fuels and fire in frequently burned longleaf pine forests. *International Journal of Wildland Fire* **18**(3), 315–325. doi:10.1071/WF08084

Hopkinson C, Chasmer L, Colin Y-P, Treitz P (2004) Assessing forest metrics with a ground-based scanning LIDAR. *Canadian Journal of Forest Research* **34**(3), 573–583. doi:10.1139/X03-225

Kennard DK, Outcalt KW, Jones D, O'Brien JJ (2005) Comparing techniques for estimating flame temperature of prescribed fires. *Fire Ecology* **1**, 75–84. doi:10.4996/FIREECOLOGY.0101075

Lefsky MA, Cohen WB, Acker SA, Parker GG, Spies TA, Harding D (1999) LIDAR remote sensing of the canopy structure and biophysical properties of Douglas-fir western hemlock forests. *Remote Sensing of Environment* **70**(3), 339–361. doi:10.1016/S0034-4257(99)00052-8

Lewis RO (1992) 'Independent Verification and Validation: a Life-cycle Engineering Process for Quality Software.' (Wiley: New York)

Loudermilk EL (2010) Linking plant demography, forest fuels, and fire in longleaf pine (*Pinus palustris*) savannas using LIDAR remote sensing and simulation modeling. PhD thesis, University of Florida, Gainesville.

Loudermilk EL, Hiers JK, O'Brien JJ, Mitchell RJ, Singhania A, Fernandez JC, Cropper WP, Slatton KC (2009) Ground-based LIDAR: a novel approach to quantify fine-scale fuelbed characteristics. *International Journal of Wildland Fire* **18**(6), 676–685. doi:10.1071/WF07138

Loudermilk EL, Cropper WP Jr, Mitchell RJ, Lee H (2011) Longleaf pine (*Pinus palustris*) and hardwood dynamics in a fire-maintained ecosystem: a simulation approach. *Ecological Modelling* **222**(15), 2733–2750. doi:10.1016/J.ECOLMODEL.2011.05.004

McNab WH, Avers PE (1994) 'Ecological subregions of the United States: section descriptions.' (USDA Forest Service: Washington, DC)

McPherson GR (1997) 'Ecology and Management of North American Savannas.' (University of Arizona Press: Tucson, AZ)

Mitchell RJ, Hiers JK, O'Brien JJ, Jack SB, Engstrom RT (2006) Silviculture that sustains: the nexus between silviculture, frequent prescribed fire, and conservation of biodiversity in longleaf pine forests of the south-eastern United States. *Canadian Journal of Forest Research* **36**, 2724–2736. doi:10.1139/X06-100

Mitchell RJ, Hiers JK, O'Brien J, Starr G (2009) Ecological forestry in the south-east: understanding the ecology of fuels. *Journal of Forestry* **107**, 391–397.

Ottmar RD, Sandberg DV, Riccardi CL, Prichard SJ (2007) An overview of the Fuel Characteristic Classification System – quantifying, classifying, and creating fuelbeds for resource planning. *Canadian Journal of Forest Research* **37**(12), 2383–2393. doi:10.1139/X07-077

Pecot SD, Mitchell RJ, Palik BJ, Moser EB, Hiers JÂK (2007) Competitive responses of seedlings and understory plants in longleaf pine woodlands: separating canopy influences above and below ground. *Canadian Journal of Forest Research* **37**(3), 634–648. doi:10.1139/X06-247

Popescu SC, Wynne RH, Scrivani JA (2004) Fusion of small-footprint LIDAR and multispectral data to estimate plot-level volume and biomass in deciduous and pine forests in Virginia, USA. *Forest Science* **50**, 551–565.

Power M (1993) The predictive validation of ecological and environmental models. *Ecological Modelling* **68**(1–2), 33–50. doi:10.1016/0304-3800(93)90106-3

Prasad A, Iverson L, Liaw A (2006) Newer classification and regression tree techniques: bagging and random forests for ecological prediction. *Ecosystems* **9**(2), 181–199. doi:10.1007/S10021-005-0054-1

Riaño D, Meier E, Allgower B, Chuvieco E, Ustin SL (2003) Modeling airborne laser scanning data for the spatial generation of critical forest parameters in fire behavior modeling. *Remote Sensing of Environment* **86**(2), 177–186. doi:10.1016/S0034-4257(03)00098-1

Riaño D, Valladares F, Condes S, Chuvieco E (2004) Estimation of leaf area index and covered ground from airborne laser scanner (LIDAR) in two contrasting forests. *Remote Sensing of Environment* **124**(3–4), 269–275.

Rykiel EJ (1996) Testing ecological models: the meaning of validation. *Ecological Modelling* **90**(3), 229–244. doi:10.1016/0304-3800(95)00152-2

Sargent RG (2005) Verification and validation of simulation models. In 'Proceedings of the 37th Conference on Winter Simulation', 4–7 December 2005, Orlando, FL. pp. 130–143. (Winter Simulation Conference: Orlando, FL)

Seni G, Elder JF (2010) Ensemble methods in data mining: improving accuracy through combining predictions. In 'Synthesis Lectures on Data Mining and Knowledge Discovery. Vol. 2.' (Eds J Han, L Getoor, W Wang, J Gehrke, R Grossman) pp. 1–126. (Morgan and Claypool Publishers: San Rafael, CA)

Smith WB, Miles PD, Perry CH, Pugh SA (2009) 'Forest Resources of the United States, 2007.' (USDA Forest Service: Washington, DC)

Su JG, Bork EW (2007) Characterization of diverse plant communities in Aspen Parkland rangeland using LiDAR data. *Applied Vegetation Science* **10**(3), 407–416. doi:10.1111/J.1654-109X.2007.TB00440.X

Vasques GM, Grunwald S, Sickman JO (2009) Modeling of soil organic carbon fractions using visible–near-infrared spectroscopy. *Soil Science Society of America Journal* **73**(1), 176–184. doi:10.2136/SSSAJ2008.0015

Wade DD, Lunsford JD, Dixon MJ, Mobley HE (1989) A guide for prescribed fire in southern forests. USDA Forest Service, Southern Region Technical Publication TP-R8–11. (Atlanta, GA)

Whelan RJ (1995) 'The Ecology of Fire.' (Cambridge University Press: Cambridge, UK)

Wing MG, Eklund A, Sessions J (2010) Applying LiDAR technology for tree measurements in burned landscapes. *International Journal of Wildland Fire* **19**(1), 104–114. doi:10.1071/WF08170

Appendix 1. Details of infrared imagery data collection and specifications for recording fire behavior

Surface temperature estimates were based on emitted infrared (IR) radiation and application of the Stefan–Boltzmann Law for a grey body emitter. Surface temperature estimates are driven by heat produced by combustion of the surface itself and by convection and radiation from nearby flames and conduction through the material itself. The detector is a focal-plane array uncooled microbolometer with 320 × 240 pixels and a spectral range of 7.5–13 μm. The S60 was fitted with a 45° lens and positioned along with the operator on a boom approximated 7–8 m above the ground and 9 m from the plot centre (view angle ~40°). The camera was positioned on the upwind side and perpendicular to a head fire so that burning fuels would be in front of unburned fuels, minimising signal dilution or obstruction. Measurements were corrected for air temperature, relative humidity and distance from target (Hiers *et al.* 2009), and emissivity was set at 0.96 (an average of live and dead vegetation, Z. Wan, unpubl. data). The estimation algorithm is robust to variation in atmospheric temperature, IR emission and IR transmittance. Thermal data were recorded at 0.25 Hz. After initial preburn images were collected of the fuel bed, the temperature range of 300 to 1500°C was chosen to capture typical longleaf fires.

Appendix 2. Date recorded and mean wind speed measured within each plot as the fire passed through

Plot	Fire group	Wind speed ($m\ s^{-1}$)	Date
1	Middle-range	1.73	23-Feb-2007
2	Middle-range	1.43	27-Feb-2007
3	Middle-range	1.26	27-Feb-2007
4	Middle-range	2.45	23-Feb-2007
5	Middle-range	1.81	23-Feb-2007
6	Middle-range	1.66	27-Feb-2007
7	Middle-range	2.88	16-Mar-2007
8	Middle-range	2.31	16-Mar-2007
9	Middle-range	1.15	27-Feb-2007
1	High-range	1.64	27-Feb-2007
2	High-range	1.41	16-Mar-2007
3	High-range	1.46	23-Feb-2007
4	High-range	2.39	27-Feb-2007
5	High-range	2.03	16-Mar-2007
1	Low-range	1.65	23-Feb-2007
2	Low-range	1.56	16-Mar-2007
3	Low-range	1.34	27-Feb-2007
4	Low-range	1.89	16-Mar-2007
5	Low-range	2.18	16-Mar-2007
6	Low-range	2.41	16-Mar-2007

Appendix 3. Burn day mean wind speed and direction from wind sensors next to each plot as well as mean temperature and relative humidity (RH) from a local weather station

Burn date	Wind speed ($m\ s^{-1}$)	Wind direction	Temperature (°C)	RH (%)	No. plots
23 February 2007	1.80	South	19.36	14.88	5
27 February 2007	1.47	South-west	22.88	42.28	7
16 March 2007	2.19	South-west	22.06	65.86	8

Appendix 4. Fuelbed (ground-LIDAR and point-intercept) metrics and fire (FLIR (forward-looking infrared)) metrics created for the CART (classification and regression trees) analysis

Metrics were determined within 33 × 33-cm cells within 20 4 × 4 -m forest plots. All height values are in metres and point-intercept data are categorical. All intensity and point density values are normalised across all plots. Fuel types were either present (1) or absent (0). sqrt, square root; qdrt, quadratic

Fuelbed metrics		Fire metrics
Ground-LIDAR	Point-intercept	FLIR
x, *y* coordinates[A]	Fuel clusters (1–11)[B]	Maximum temperature °C
Mean height	Fuel types (0 or 1):	90th quantile temperature °C
Maximum height	1- and 10-h fuels (10 h)	Residence time above 300°C
Variance of height	100- and 1000-h fuels (100 h)	Residence time above 500°C
Kurtosis of height	Pine litter	
Skewness of height	Oak litter	
Height distribution ratio (mean/maximum)	Perched pine litter	
Sum of heights	Perched oak litter	
Spread of heights (maximum – minimum)	Wiregrass	
Point density (0–1)	Other grasses	
Mean LIDAR intensity (0–1)	Forbs	
int_{sqrt} (sum of sqrt(LIDAR intensity))	Shrubs	
int_{qdrt} (sum of qdrt(LIDAR intensity))	Volatile shrubs	
int_{lnr} (sum of LIDAR intensity)	Bare soil (no vegetation or fuel)	

[A]Used for plot-level analysis only; [B]used for multiplot (e.g. grouped) analysis only.

Appendix 5. Results of *CART* (classification and regression trees) analysis at the collective plot level (all plots together) using the 10-fold cross-validation procedure

Residence times (T300, T500) are in number of 4-s intervals. Response variables are the fire metrics, namely Tmax, maximum temperature (°C); Q90, 90th quantile temperature (°C); T300, residence time above 300°C; and T500, residence time above 500°C. T_n, no. of terminal nodes; CVRE, cross-validation relative error; RRE, resubstitution relative error; R^2, coefficient of determination; RMSE, root-mean-square error; RPD, residual prediction deviation

Response variable	T_n	CVRE	RRE	R^2	RMSE	RPD
Collective data (20 plots, $n = 3380$)						
Tmax	330	0.540	0.124	0.43	64.37	1.24
Q90	322	0.390	0.090	0.22	63.62	1.11
T300	323	0.317	0.062	0.54	1.91	1.46
T500	341	0.296	0.063	0.38	1.61	0.90